JOURNAL OF MATERIALS SCIENCE 32 (1997) 4941–4955

Micromechanical analysis of the finite element calculation of a diffusional transformation

J. F. GANGHOFFER
ICSI. 15, Rue Jean Starcky. B.P. 2478. 68057 Mulhouse Cedex, France

S. DENIS, E. GAUTIER
LSG2M. Parc de Saurupt. 54042 Nancy Cedex, France

S. SJÖSTRÖM
Department of Mechanical Engineering, Linköping University, 58183 Linköping, Sweden

A micromechanical model of a diffusional transformation has been developed, which describes the progress of the transformation within a three-dimensional ''unit cell'' submitted to an external stress state. The example chosen is that of an isothermal pearlitic transformation of a steel. The transformation plastic strain is due to interactions occurring between the local stresses and the transformation process, resulting in an oriented plastic flow in or in the vicinity of the material layers swept by the transformation front. The analysis of the local mechanical states of the simulation provides a good interpretation of the evolution of transformation plastic strain, when considering the effect of applied stress level and the way mechanical properties are imposed on the newly formed phase. In particular, the normality law for transformation plasticity is related to the shape of the local plastic zones. The discrepancy observed between simulation and experience is then discussed, following two main points: the influence of the behaviour law of the phases and the way interactions between neighbouring cells are prescribed. The difficulty and importance of obtaining realistic mechanical properties of the forming pearlite is pointed out.

1. Introduction

Transformation plasticity occurs when a material undergoes a transformation of its microstructure under the simultaneous influence of an applied load. Experimentally, the phenomenon and its mechanisms have been extensively described in Gautier *et al.* [1] and modelled from a phenomenological point of view by Denis *et al.* [2]. At the scale of the phases, a micromechanical model using a finite element (FE) simulation has been developed by the present authors [3, 4], describing a transformation occurring with nucleation and growth inside a "unit cell" submitted to an external stress state. In that case, the mechanism responsible for transformation plasticity is an orientation of the plastic flow generated around the new phase particles by the local stress state.

In a previous paper [3], both the models set up for describing the transformation and the evolutions of transformation plasticity versus the progress of the transformation were presented. Mainly, the influence of parameters inherent to the FE discretization was studied, considering a uniaxial applied stress of a constant magnitude. In the continuation of that paper [4], the model was submitted to complex loadings, uniaxial stress states of different magnitudes and histories and multiaxial stress states, resulting in the formulation of a constitutive law for transformation plasticity.

In parallel to the behaviour exhibited at the scale of the cell, the transformation induces local effects arising from the imposed transformation strain, which interacts with both applied and local stress states. Such a simulation is then the more interesting as it provides access to the development of plastic zones formed around the newly formed phase particles and to the variations of local mechanical quantities, i.e. defined at the scale of the phases. Therefore, it is possible to go deeper into the analysis of the local effects of the transformation, than an experimental set-up or analytical models (often based on a simplified hypothesis, such as uniform strain rates [5], or uniform stress rates [6]) would allow, for which the analysis of such a local information is more problematic.

In the present work, we investigated first the local origin of transformation plasticity, by studying the variation of defined mechanical parameters on some restricted geometrical entities located within the cell. The analysis was led for a constant uniaxial applied stress and the influence of some parameters of the simulation on the local strain and stress fields has been pointed out. Focus was mainly on the spherical growth model, because the analysis of local fields is more complex for the random description due to the topology of the transformation front; therefore, only

0022–2461

a few elements are given for this second model. The model had been discussed on the basis of the comparison between experience and simulation. First, a short review of both transformation descriptions is presented and the parameters used in the analysis of the local mechanical states of the simulation are introduced.

2. Local origin of transformation plasticity

Because the model has been thoroughly presented elsewhere [3], we recall briefly its essential features. The transformation progress is described within a three-dimensional "unit cell" (a cube) submitted to an external stress state. Each element of the FE mesh within the cell corresponds to a volume element of either phase provided with specific mechanical properties, and its transformation is simulated by the affectation of an isotropic transformation strain and new mechanical properties; this procedure ends when the whole cell is filled with pearlite. The mechanical properties are given to an element either at the beginning of the transformation (before the element receives its transformation strain), or just after the transformation. The first situation will be labelled "beg" and the second "end" in the sequel. At the scale of the cell, transformation plasticity is due to the local accommodation of the imposed transformation strain, i.e. the plastic flow generated around the pearlite particles induces a macroscopic plastic flow "oriented" by the external load. We first consider an elastoplastic behaviour law of the phases, with isotropic hardening; the corresponding mechanical properties are given in Table I.

Because the transformation occurs by nucleation and growth, we have described the transformation progress in two different ways, corresponding to two different scales.

1. a spherical growth model describing the simultaneous growth of regularly disposed nuclei. The transformation starts by the first element located in the corner of the mesh and proceeds by the formation of the successive surrounding elements layers. Owing to the spherical geometry of the growth, only one octant of the cell is considered. The periodicity of the distribution of pearlite particles and interactions between neighbouring cells are simulated by prescribing the faces of the cell to remain plane and parallel during the transformation. The transformation front consists, in this case, of the "spherical" boundary surface separating the elements already transformed, i.e. those which have received their transformation strain, from those still in the austenitic phase;

2. a random progression model in which the pearlite particles appear in their definite size, considering the growth as a hidden phenomena: transformation proceeds in that case by the random formation of pearlite elements. Because this model describes the transformation on the macroscopic scale of a sample, there is no influence of the kind of boundary conditions applied on the cell (which can be either those of the spherical growth model or of free type). Owing to the randomness of the model, there is in this case no simple identification of the front, which is discontinuous practically all along the transformation, because different aggregates of pearlite particles are almost always separated by mother phase particles.

2.1. Definition of mechanical parameters and analysis loci

Among the local results of the simulation, the development of plastic zones is of a prominent interest for the analysis of the local effects of the transformation. The parameter used below to quantify this information is the equivalent cumulated plastic strain, denoted ε_p. For a diffusional transformation, transformation plasticity is a reflection of the "classical" microplasticity developed around newly formed phase particles. However, a scalar measure of the local plasticity as defined above is insufficient for explaining the development of transformation plasticity at the macroscale, because it originated in a local plastic flow oriented by the internal stress state. Transformation plasticity depends also on the orientation effect of the external stress: no plastic flow is observed at the scale of the cell for no applied load, even if plastic flow appears locally. This is due to an isotropic accommodation of the local plasticity, on average. It is deduced that transformation plasticity is due to a microplasticity which is favourably oriented by the external stress.

In order to quantify the influence of both external and local stress states on the orientation of the local plastic flow, we introduce a parameter, called the anisotropy factor, η, in the following, and defined as the contracted product of the local stress deviator $\boldsymbol{\sigma}_d$ by the applied stress deviator $\boldsymbol{\Sigma}_d$. We divide by the product of norms to obtain a factor normed to unity (η lies between -1 and 1)

$$\eta = 3/2\boldsymbol{\sigma}_d : \boldsymbol{\Sigma}_d / J2(\boldsymbol{\sigma})\, J2(\boldsymbol{\Sigma}) \qquad (1)$$

Because the local plastic strain rate tensor also has the same principal directions as the local stress deviator (from the normality rule), a unit value for η (-1 or 1),

TABLE I Input data for the FE calculation

Phase	Young's modulus (MPa)	Poisson's ratio	Yield strength (MPa)	Hardening slope (MPa)
Austenite	137 500	0.3	25	3800
Pearlite	137 500	0.3	110	8300
Volume change 3.6×10^{-3}				

obtained when both stress tensors have the same principal directions, reflects a strong influence of the external load on the orientation of the local plastic flow (it leads effectively to a macroscopic plastic strain which is the more favourably oriented in the principal directions of $\boldsymbol{\Sigma}$). Conversely, a small value for η means a weak interaction between both entities. We note that Leblond [5] has used the same parameter in order to assess the validity of an analytical model for transformation plasticity.

In addition to these two parameters which enable more specifically to correlate the passage of the transformation front with the development of transformation plasticity, we study in some cases the evolutions of the hydrostatic stress, σ_h, which quantifies the compression state accompanying the passage of the front (and its transition to traction afterwards) and of the equivalent stress, σ_e, which measures the transition from elastic to plastic states, as well as hardening.

For the spherical growth model, we consider meshes of 10 linear elements; the transformation proceeds, therefore, by the successive formation of an equal number of layers of elements within the cell. Owing to the spherical geometry of the growth, the cell contains the principal diagonal as a privileged axis (it plays the role of a time axis, because it allows the degree of progress of the transformation inside the cell to be marked), which is normal to the moving front. Most of the analysis will therefore be followed for the diagonal nodes, which we label *iii* (*i* ranging from 1–10). We can note, however, that the application of an uniaxial load breaks this symmetry. More generally, a node inside the mesh is labelled *ijk*, where the indices correspond to the axes z, y, x, respectively (Fig. 1).

Considering now the random progression model, for a typical mesh of 4 linear elements, the transformation consists of 64 steps. Because the cell represents, in that case, the whole sample, there is no natural symmetry and it is therefore necessary to follow the evolutions of the local parameters in the vicinity of a given node. The nodes within the cell are labelled in the same way as is done for the spherical growth model (Fig. 2).

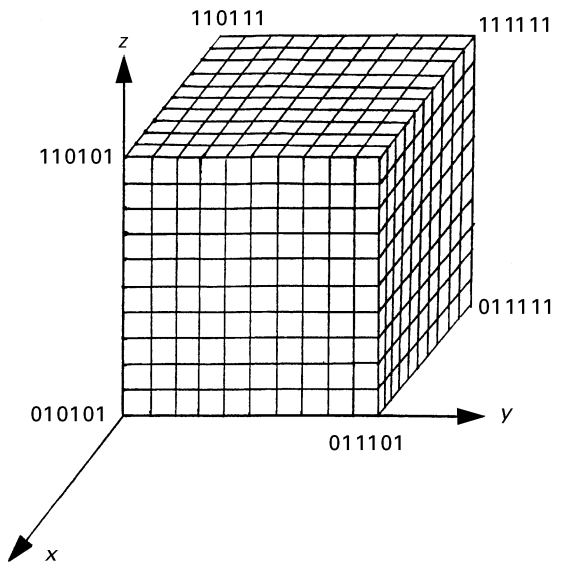

Figure 1 Spherical growth model: 10 10 10 mesh. Unit cell.

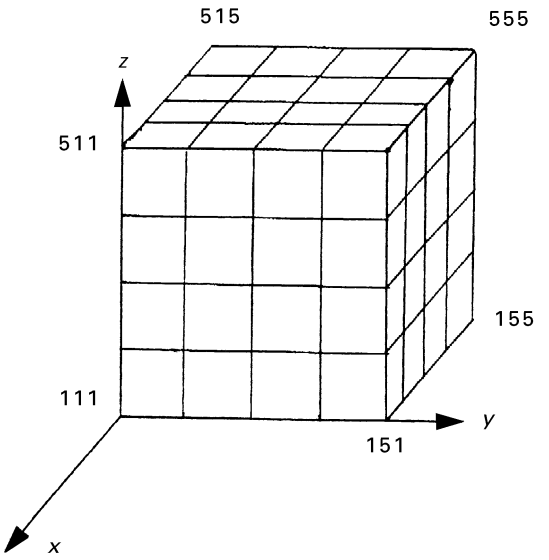

Figure 2 Random growth model, 4 4 4 mesh. Unit cell.

In the following sections, we analyse the influence of the magnitude of the external load and of the way mechanical properties are imposed to the new phase on the evolutions of the previously defined local parameters. Owing to the irregularity of the transformation front for the random progression model, most of the analysis will be devoted to the spherical growth model.

2.2. Spherical growth model

2.2.1. Effect of the magnitude of an external uniaxial stress

The case with no applied load provides a first insight into the local effects of the transformation. Figs 3 and 4 show the evolutions of ε_p and σ_h for the diagonal nodes, respectively; the transformation progress is described by the transformation step in order to obtain a correct scaling of the results for the first fractions (the fifth step represents a transformed fraction of only 12.5%). Mechanical properties are imposed at the "end" of each step to the forming particles, and we consider simulations in which the new phase does not inherit the memory of plastic strain accumulated previously in austenite.

Following the evolution of ε_p for these nodes makes a gradual plastification apparent with the transformation progress. In order to obtain a clearer analysis, we reduce the information to the nodes 3 3 3, 5 5 5, 7 7 7, 9 9 9 and 1 1 1 1 1 1. For instance, node 5 5 5 is little plasticized until step 3. Most of its plastification occurs then between steps 3 and 5 when the node is swept by the front; a quite fast saturation of local plasticity occurs afterwards, because the node then has the higher mechanical properties of pearlite and a slight plastic flow increase is then observed in the

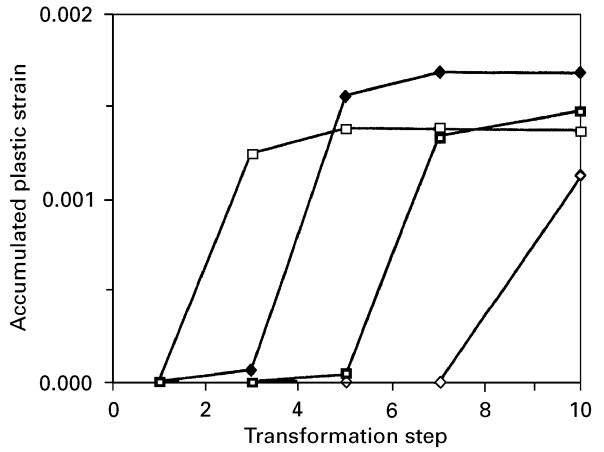

Figure 3 Spherical growth model, no applied stress. Evolution versus transformation progress of the accumulated plastic strain for the diagonal nodes: (□) 3 3 3, (◆) 5 5 5, (■) 7 7 7, (◇) 9 9 9.

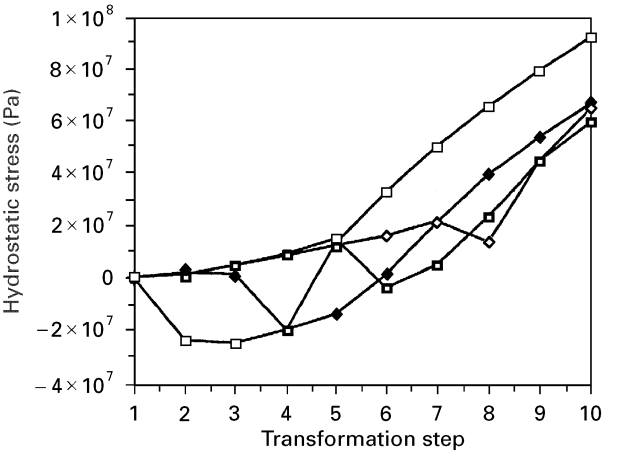

Figure 4 Spherical growth model, no applied stress. Evolution versus transformation progress of the hydrostatic stress for the diagonal nodes: (□) 3 3 3, (◆) 5 5 5, (■) 7 7 7, (◇) 9 9 9.

pearlitic regions. One deduces from the unloaded case that most of the plastification occurs "during" the passage of the front, when the material still has the mechanical properties of austenite.

The later occurrence of the transformation in the elements layer located near the external boundary of the cell leads to a weaker plasticity for the corresponding surface nodes (ε_p is nil for node 11 11 11). The levels reached are, however, comparable for "internal" nodes (e.g. node 3 3 3) and "external" nodes (e.g. node 7 7 7) and are of the order of 10^{-3} to 1.7×10^{-3}; as expected, the highest levels are obtained for nodes located in the centre of the cell (e.g. node 5 5 5).

No macroscopic plastic flow is observed at the scale of the cell, even if a quite important microplasticity develops at the local level. This can be attributed to an isotropic plastic flow pattern around the forming particles, leading globally to a nil transformation plastic strain. In order to assess this feature, we examine the shape of plastic zones by considering the cumulated equivalent plastic strain for nodes located in a plane perpendicular to the diagonal of the cube: such a plane is defined by the equation $x + y + z = k$, in which k is the distance from the plane to the origin. For a node located in this plane (having indices i,j,k), all nodes obtained by a permutation of the indices (for instance nodes 3 4 5, 3 5 4, 4 3 5, 4 5 3, 5 4 3, 5 3 4) are equidistant to the diagonal and belong therefore to a "circle". For such a set of nodes, we have checked that ε_p is identical, which confirms the isotropic character microplasticity for an unloaded cell.

The effect of the transformation on local stress variations is reflected by the passage of a node from traction to compression when it is swept by the front (Fig. 4). The hydrostatic stress drops suddenly when the node is affected by the transformation, becomes negative and the node then goes back to traction (e.g. node 7 7 7 is under compression at step 6 for which $\sigma_h = -10$ MPa and reaches the "end" of the transformation at $\sigma_h = 60$ MPa). The later transformation of the nodes located near the outer surface (which we call "external" nodes here) of the cell leads for them to a drop of σ_h during which the material retains its traction state (this is the case for node 9 9 9).

We now consider loaded cases (for which a transformation plastic strain develops) and study the effect of the magnitude of the applied load on the development of local plasticity. We pay attention to the case of a 20 MPa applied load, with properties imposed at the end of the transformation step (Fig. 5a). As for the

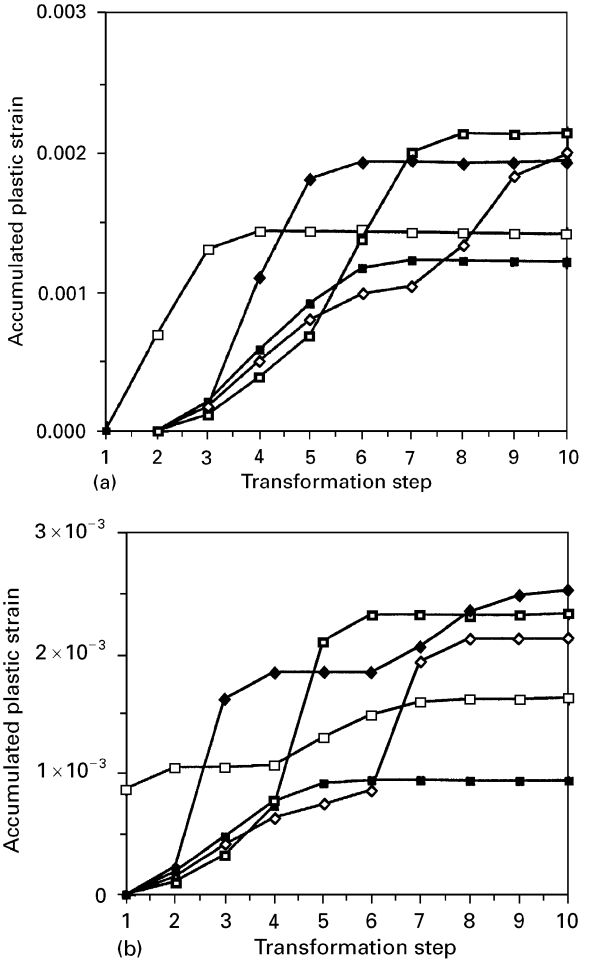

Figure 5 The spherical growth model at an applied stress of 20 MPa: (a) "end" and (b) "beg" cases. Evolution versus transformation progress of the accumulated plastic strain for the diagonal nodes: (□) 3 3 3, (◆) 5 5 5, (■) 7 7 7, (◇) 9 9 9, (■) 11 11 11.

unloaded case, the microplastification occurs mainly during the passage of the front, in the austenitic regions and in the forming zones. A first noticeable effect of the applied load is to increase globally the plastification level; this feature is more pronounced for nodes transforming in a later stage: for instance, quite similar evolutions of ε_p are observed for node 3 3 3 (compare the evolution of ε_p in the unloaded and the loaded cases, Figs 3 and 5, respectively), but the levels are sensibly different for node 5 5 5 ($\varepsilon_p = 1.7 \times 10^{-3}$ in the unloaded case, $\varepsilon_p = 2 \times 10^{-3}$ for 20 MPa).

The difference between both cases is particularly marked for the "external" nodes: application of the 20 MPa load level leads to a plastification of these nodes well before the passage of the front (nodes 7 7 7, 9 9 9, 11 11 11 are plasticized already at step 2). It results in ε_p levels much higher for these nodes ($\varepsilon_p(9\,9\,9) = 1.1 \times 10^{-3}$ for no applied load, and $\varepsilon_p(9\,9\,9) = 2 \times 10^{-3}$ for 20 MPa). This early plastification (from step 3 corresponding to a transformed fraction of 2.7%) of "external" nodes is more clearly visualized on Fig. 6b which shows the distribution of ε_p along the diagonal for steps 3, 5, 7, 10; we compare this distribution to the one obtained for half that load (10 MPa) on Fig. 6a. Indeed, one observes in this last case a gradual

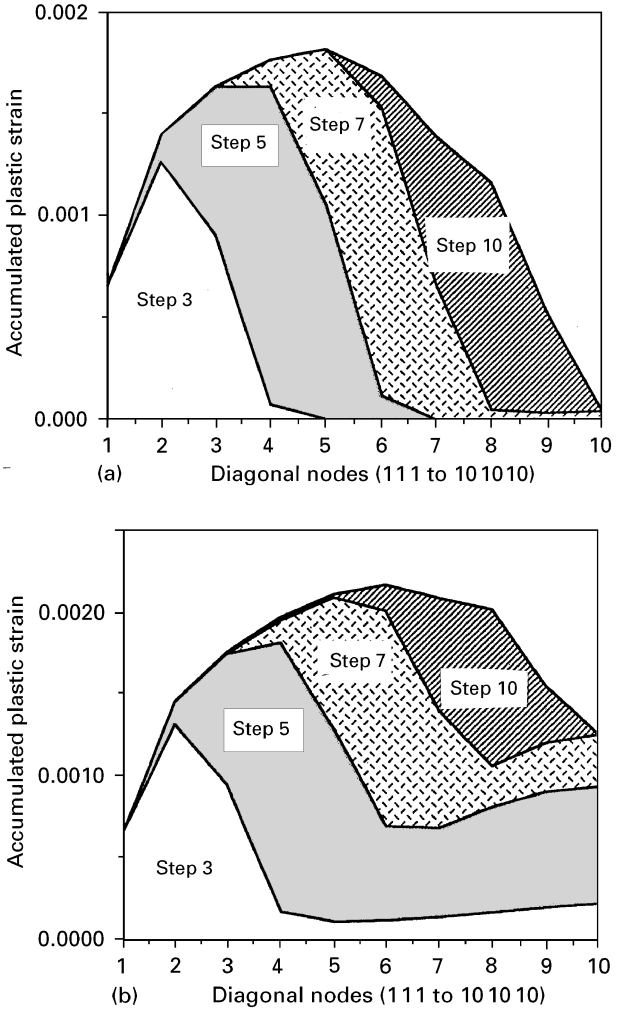

Figure 6 Spherical growth model, for an applied stress of (a) 10 MPa and (b) 20 MPa, "beg" case. Evolution versus transformation progress of the accumulated plastic strain for the diagonal nodes.

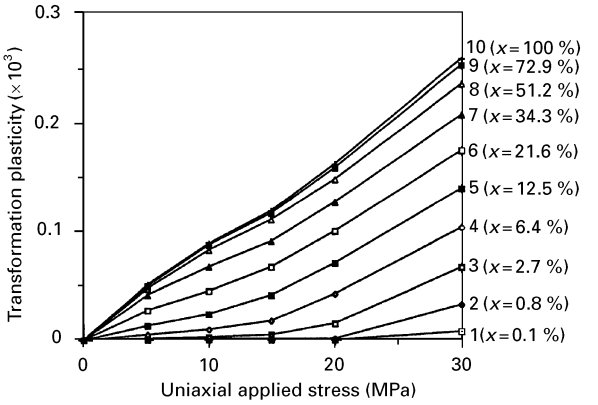

Figure 7 Evolution versus uniaxial stress level of transformation plasticity; x = transformed fraction.

development of microplasticity along the diagonal, because the increase of ε_p occurs mainly when the node is swept by the front (e.g. node 4 4 4 is nearly elastic at step 3 and little plasticity develops after step 5).

Opposite to this, for an applied load of 20 MPa, "external" nodes plastify from the very beginning of the transformation (third step), as shown in Fig. 6b, resulting also in a more uniform plastic flow pattern within the cell. The plastification of "external" layers increases markedly with the transformation progress, contrary to the case of 10 MPa. This change of plastic pattern when increasing the load (from 10–20 MPa) can be correlated to the change of slope observed (between 10 and 20 MPa; more obviously in the early stage of the transformation) in the evolution of the transformation plastic strain versus the amplitude of the applied load (Fig. 7).

For the unloaded case, the shape of the plastic zones (for 20 MPa) is analysed: considering also the plane normal to the diagonal, identical ε_p values are obtained for nodes having their first and second index permuted, which evinces the symmetry of the plastic flow with respect to the plane $y = z$. The same symmetry is observed for the external stress deviator (because the load Σ is applied in the x-direction, the y and z components of the stress deviator are equal to $-2/3\Sigma$). This result is a local explanation of the fact that the transformation plastic strain and the external stress deviator have the same principal directions.

2.2.2. Effect of the way mechanical properties are imposed on the new phase

We analyse in the following the effect of the way of imposing the mechanical properties on the new phase. A uniaxial external stress of 20 MPa is considered and we compare the evolution of the cumulated equivalent plastic strain versus transformation step for the diagonal nodes, in both cases ("beg" case, Fig. 5b; "end" case, Fig. 5a).

Local plasticity develops quite differently in each situation: the increase of ε_p for a diagonal node is smaller when it is swept by the front in the "beg" case

(as can be seen, for instance, for node 5 5 5 between steps 4 and 5) and most of the local plasticity develops here before and after the passage of the front. This is confirmed, for instance, by the fact that node 7 7 7 experiences the highest increase of ε_p between steps 4 and 5 (it is then in the austenitic state); a smaller increase is noticed for node 3 3 3 which is already transformed and has therefore the high mechanical properties of pearlite. Following the evolution of ε_p for node 5 5 5, a first important increase occurs between steps 2 and 3, followed by a smaller one between steps 3 and 4. A saturation effect appears during the passage of the front (ε_p is constant between steps 4 and 6), followed by a second and smaller increase until the end of the transformation.

These differences in the behaviour can be explained by the high properties of a node under transformation in the "beg" case; it is therefore more difficult for the transforming layer to deform plastically and it is the surrounding area that accommodates the transformation strain, essentially those layers which are still austenitic. On the contrary, the transforming layers experience the highest plastification in the end case, because the corresponding elements have the properties of austenite. This explains the difference in the occurrence of microplasticity and particularly the fact that the second plastification observed in the "beg" case is less marked, because it concerns layers of elements in the pearlitic state. For the nodes located near the outer boundary, there is only one plastification and ε_p remains constant thereafter.

It is interesting to note the development (even small) of local plasticity in the pearlitic regions (in the "beg" case), which was not considered, for instance, in the models developed by Leblond [5]; the author considers that the new phase inherits the plastic strain developed in the mother phase before transformation, but no plastic flow could appear afterwards. However, this hypothesis is reasonable regarding the results of our simulation, because rather little plastic flow develops in pearlite and the main source of microplasticity comes from plastic flow of the mother phase.

The effect of the transformation on local stress variations is evinced by the evolutions of the hydrostatic (Fig. 8) and equivalent stresses (Fig. 9) ("beg" case). The passage of the front leads to a transition to compression for the corresponding nodes (Fig. 8). One can note that the plastification of the nodes located in austenite occurs essentially under traction; their second plastification occurs also under traction. A second effect of the front passage is a drop of the equivalent stress (Fig. 9). The initial value of σ_e is very near the external stress level (20 MPa) and the levels are quite near 25 MPa in the regions which plastify (e.g. for node 5 5 5 at steps 3, 4, 5). The stress levels reached at the end of the transformation are near the external stress for the "external" nodes and they range between 80 and 100 MPa for "internal" nodes. In reality, stress levels obtained at the Gauss points are higher than the pearlite yield strength (110 MPa), because the corresponding nodes experience a (small) plastification when they are already transformed, as shown in Fig. 5b. The reason for this discrepancy is that nodal

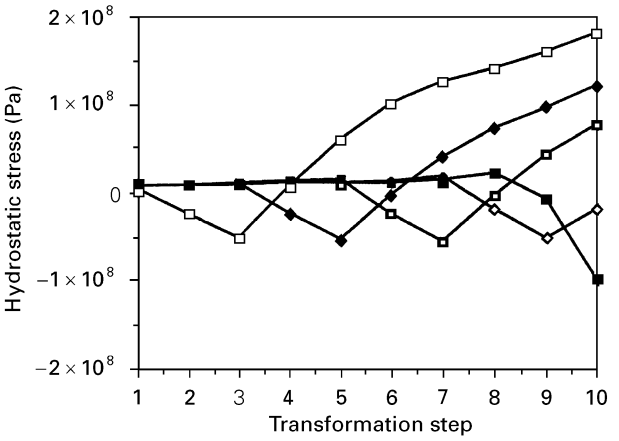

Figure 8 Spherical growth model for an applied stress of 20 MPa: "beg" case. Evolution versus transformation progress of the hydrostatic stress for the diagonal nodes: (□) 3 3 3, (◆) 5 5 5, (◘) 7 7 7, (◇) 9 9 9, (■) 11 11 11.

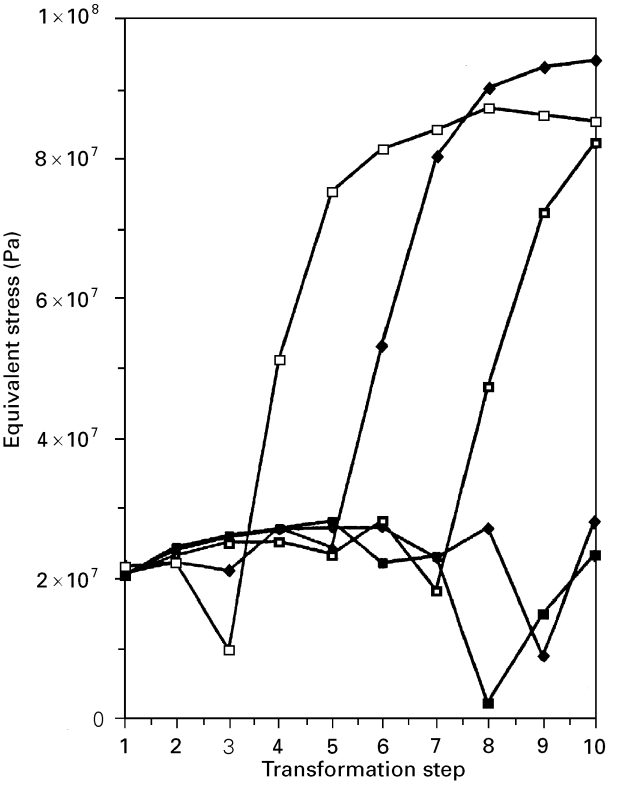

Figure 9 Spherical growth model for an applied stress of 20 MPa: "beg" case. Evolution versus transformation progress of the equivalent stress for the diagonal nodes: (□) 3 3 3, (◆) 5 5 5, (◘) 7 7 7, (◇) 9 9 9, (■) 11 11 11.

results of the FE calculations are averaged over the elements sharing the node.

The "beg" case leads to ε_p values higher than those obtained in the "end" case; this tendency seems to contradict the induced evolutions of the transformation plastic strain. This can be attributed to the insufficiency of the mere parameter ε_p to account for the local interactions between the transformation strain and the local stresses, leading to an orientation of microplasticity. We therefore need to consider, in addition, the evolutions of the anisotropy factor, η,

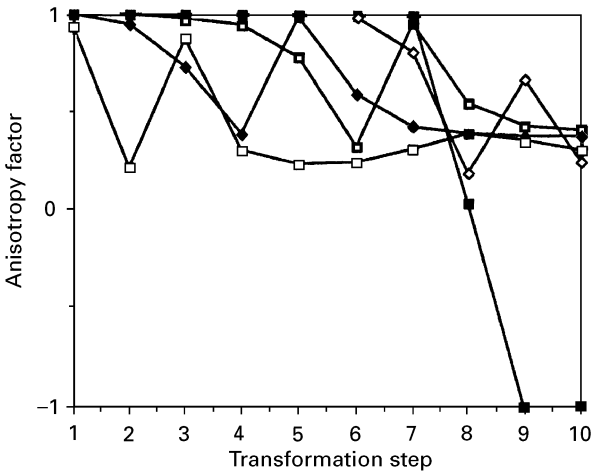

Figure 10 Spherical growth model for an applied stress of 20 MPa: "beg" case. Evolution versus transformation progress of the anisotropy factor for the diagonal nodes: (□) 3 3 3, (◆) 5 5 5, (◘) 7 7 7, (◇) 9 9 9, (■) 11 11 11.

which provides a measure of the orientation effect of local plastic flow. We consider these evolutions in the "end" case (Fig. 10). For a given diagonal node, η is equal to unity in the beginning of the transformation, drops when the node starts to plastify and tends to unity during its transformation (e.g. node 5 5 5 at step 5); after transformation, η drops again to lower values. There is consequently a strong orientation effect of microplasticity generated for the material layers swept by the front.

The situation is different for the "beg" case, because the passage of the front does not generate plastic flow in the layer of elements undergoing the transformation. In that case, there is a well-oriented ($\eta = 1$) plastic flow of the austenitic layers located near the front; the second plastification of the layers already transformed is much less oriented and contributes very little to macro-plasticity. Consequently, it is the comparison between both cases ("beg"/"end"), of the levels of local plastic flow generated just after the passage of the front which provides elements for explaining the sense of the induced evolutions of transformation plasticity. Indeed, considering nodes 3 3 3, 5 5 5, 7 7 7 at steps 3, 5, 7, respectively (Fig. 5a, b), the highest plastic flow levels are obtained for properties imposed at the end (e.g. for node 3 3 3 with $\varepsilon_p = 1.1 \times 10^{-3}$ in the "beg" case; $\varepsilon_p = 1.4 \times 10^{-3}$ in the "end" case).

We conclude from the analysis of the local mechanical states for the spherical growth model that the local origin of transformation plasticity is a microplasticity experienced by the transforming layers and of those located around the front when properties are imposed at the end of the transformation step; the contribution of the other layers to transformation plasticity is quite small, because they experience a local plastic flow either quite small or isotropic.

2.3. Random progression model

Owing to the absence of a regular and continuous transformation front, a systematic analysis of the local results of the simulation would be quite untractable and we therefore make a more punctual analysis of the evolutions of the mechanical parameters. We consider a mesh of 4 linear elements and an external uniaxial load of 10 MPa. The transformation consists of 64 steps and we select the local information of each of 8 steps: a linear interpolation is then done between them in order to obtain a relatively continuous evolution of the parameters. The local analysis is focused on some nodes chosen regarding their position inside the cell: the nodes 5 5 5 and 5 5 3 located on the outer boundary of the cell and node 3 3 3 located in the centre of the cell. In Fig. 11, we visualize the transformed zones (hatched areas) between steps 25 and 32 in planes perpendicular to the z-axis, corresponding to the different layers of nodes; elements transforming at step 32 (half-transformation) are cross-hatched. Fig. 12a, b shows the evolutions of ε_p versus transformation step for nodes 5 5 5 and 5 5 3 in the "beg" and "end" cases, respectively. A strong increase of ε_p occurs for node 5 5 5 between steps 24 and 32 when the corresponding element (located in the corner of the cell) transforms; afterwards (after step 32), the increase of ε_p is very weak due to the high mechanical properties (those of pearlite) of the environment of the node. Considering now node 5 5 3, the evolution of ε_p has the same form: a strong increase occurs between steps 24 and 40, followed by much smaller variations. One can notice that node 5 5 3 (common to two elements) experiences the transformation the first time at step 40; therefore, the increase of ε_p between steps 24 and 32 is due to the transformation of neighbouring elements containing this node (on layers 3 and 4, Fig. 11).

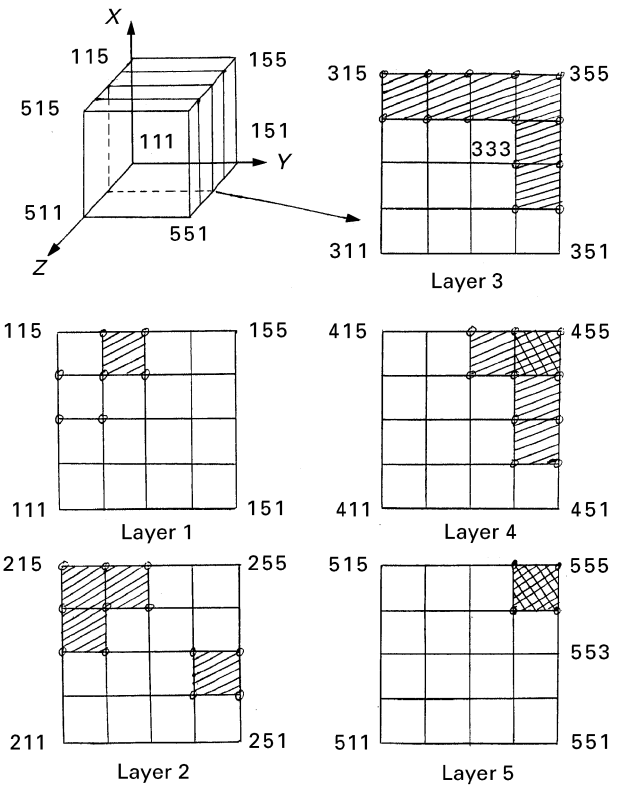

Figure 11 Random growth model. Transformed zones between steps 25 and 32 (hatched areas); cut perpendicular to the z axis.

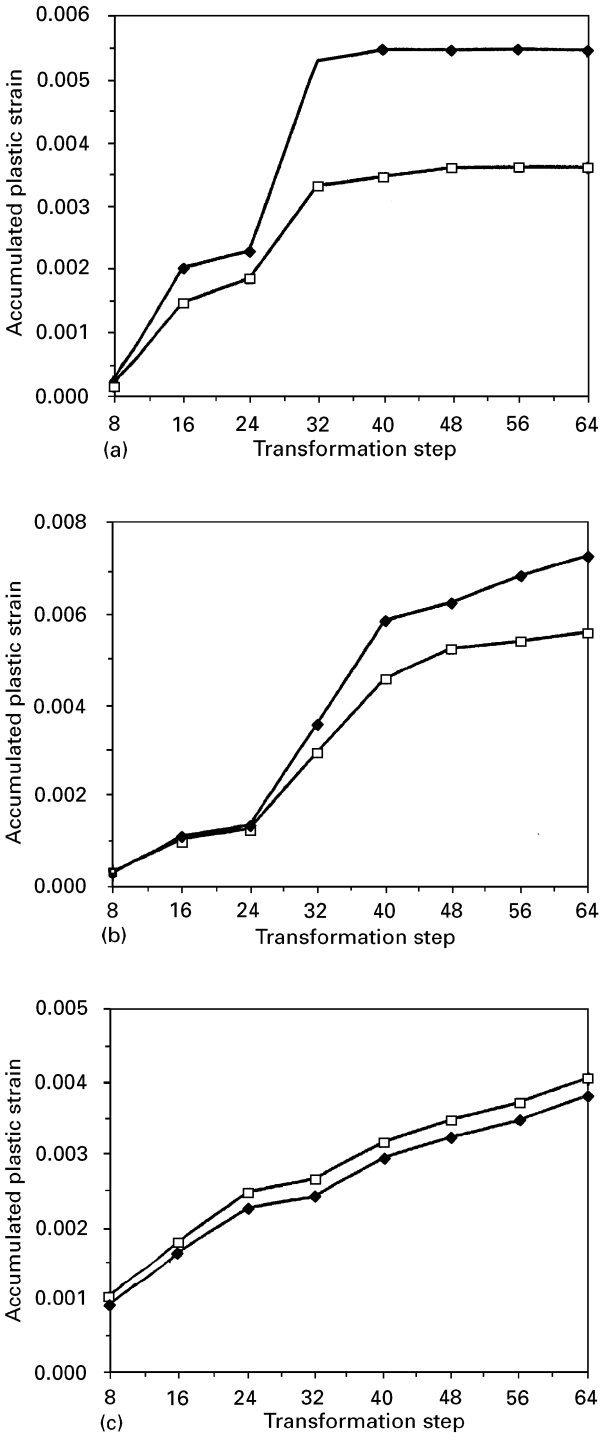

Figure 12 Random growth model for an applied stress of 20 MPa: (□) "beg" and (◆) "end" cases. Evolution versus transformation progress of the accumulated plastic strain for nodes (a) 5 5 5, step 32, (b) 5 5 3, step 40, and (c) 3 3 3, step 6.

The same behaviour has been observed for other nodes of the mesh located near the boundary. Considering now "internal" nodes, there is a more linear evolution of ε_p. For instance, node 3 3 3 undergoes the effect of the transformation for the first time at step 6; it experiences plastic flow until the last step due to the successive transformation of the environment (node 3 3 3 is common to 8 elements). However, the plastic flow level reached at the "end" of the transformation is weaker than that obtained for "external" nodes.

These results show that the plastification of a node has principally three origins: the transformation of the far-located environment when the node is still austenitic, the transformation of the near-located environment (there is still austenite around the node) and its own transformation.

The affectation of mechanical properties at the beginning of the transformation step leads to less local plastic flow than in the "end" case; this tendency is particularly marked for the "external" nodes; considering, for instance, node 5 5 5, the increase of ε_p during the transformation (between steps 24 and 32, Fig. 12a) is 0.003 in the "end" case, and only half of that (0.0015) in the "beg" case. However, at the scale of the cell, the resulting effect on transformation plasticity is weak [3]: for a given element under transformation, it seems that the main contribution to transformation plasticity arises from the plastification of its environment (near or far); as for the growth model, the local plastic flow generated is strongly oriented towards the load direction.

Compared to the spherical growth model, the random formation of pearlite leads to a more uniformly distributed plasticity within the cell (we checked that all nodes are already plastified at step 8, corresponding to 12.5% transformed fraction). Globally, this leads to much higher plastic levels (they can reach 0.8%) for the random model; however, because the increase of microplasticity is confined in a much smaller volume (only one element transforms at each step) compared to the growth model (in the case, a full layer of elements transformed at each step), the resulting effect on transformation plasticity is much weaker [3].

For the growth model, we observe that the increase of plastic flow consecutive to the transformation of a node occurs on material elements under compression.

To conclude this part, one can first note the difficulty of making a systematic and rigorous analysis of the correlation between the local mechanical states and transformation plasticity, due mainly to the large amount of informations that one should handle in the ideal case; a second reason is the complexity of building macroscopic (i.e. at the scale of the cell) plastic potentials, which makes it difficult to quantify the correlation. The analysis was therefore restricted to a relatively limited information for each model, the generalization being more easy in the growth case due to the directionality of the transformation.

Notwithstanding these difficulties, the local analysis is interesting in itself, because it provides an insight into a further scale level (localization of plastic deformations in each phase, orientation of microplasticity, local stresses generated during the transformation progress), which analytical models or experimental techniques access less easily This gives a further interest of using a micromechanical approach.

The next section is devoted to the discussion of the model, relying on the comparison between results of the simulation and experience; local results will be used for a better understanding of the evolutions of transformation plasticity.

3. Discussion of the model

Fig. 13 shows the evolutions (versus transformed fraction) of transformation plastic strain for both models (uniaxial load of 20 MPa), to which the experimental evolution is superposed. There is an effect of the way mechanical properties are imposed on the new phase for the growth model, due to the still over-sized last transformation steps [3]; however, a good agreement is found between both models when properties are imposed at the "end". This tends to prove that both models, even if they describe the physical reality at different scales, represent the same behaviour of the material at the macroscopic scale.

However, the parabolic shape obtained for the simulation is not adequate for representing the actual behaviour, as measured on a sample: transformation plasticity develops there very regularly and the evolution is nearly linear. Strong differences appear after half-transformation and transformation plasticity calculated for the complete transformation is smaller than the experimental measure. Considering the reliability of experimental measurements, one can point out the difficulty of obtaining experimental points for a partial transformation (the uncertainty concerning the amount of pearlite is about 10%); nevertheless, the value of transformation plasticity obtained for a complete transformation has been confirmed by numerous experiments and the order of magnitude by many authors [2].

In order to go deeper into the analysis of this discrepancy, we studied successively the influence of the behaviour law of the phases introduced in the simulation and that of transition from the micro- to the macro-scale, i.e. the way interactions between neighbouring cells are described.

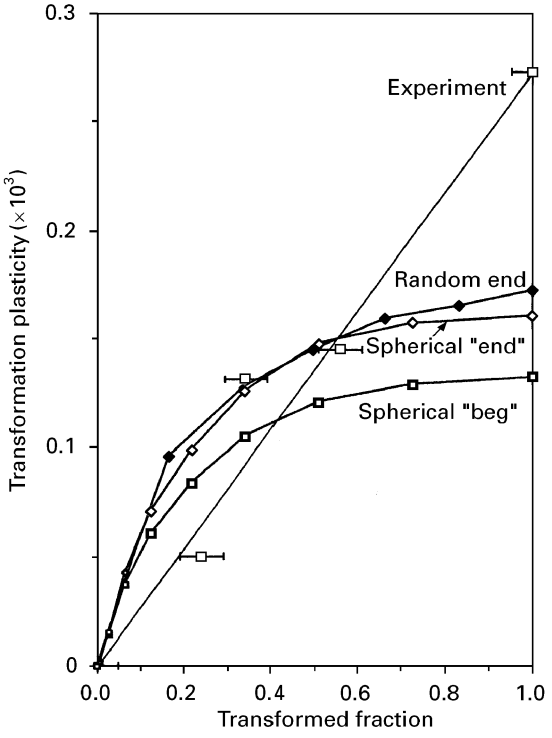

Figure 13 Evolution versus transformation progress of transformation plasticity for both models. Comparison between simulation and experiment.

3.1. Influence of the behaviour law of the phases

In the model, we considered an elastoplastic behaviour law of the phases with isotropic hardening. With respect to this assumption, two points can be considered:

1. the conservation of plastic strain memory implies that the new phase is consolidated by the totality of plastic strain developed in austenite, which certainly does not reflect the true behaviour. Several authors have used hardening models in which the new phase is only partially consolidated by the plastic strains of the mother phase [2, 7];
2. due to the high temperature of the transformation (675 °C), both phases have a viscous behaviour. In order to study this effect, we considered simulations with an additional creep deformation in the behaviour law of the phases.

3.1.1. Effect of plastic strain memory

From the point of view of the calculation, the subtraction of the memory of plastic strain is equivalent to changing the reference state used for measuring the equivalent cumulated plastic strain of any integration point, when it is transformed into the new phase. The value obtained just before the transformation then serves as a new reference, which means that the point has effectively a yield stress equal to the pearlite yield strength when it is converted to pearlite.

We show in Fig. 14 the evolution of transformation plasticity for both models (uniaxial load of 20 MPa) considering both possibilities for each (subtraction or not of plastic strain memory). For the growth model, there is a relatively weak effect of memory, with a maximum of about 10% at the "end" of the transformation. The effect is much more marked for the random model, because the discrepancy increases with the transformation progress until 25% at the "end". Considering the situation in which one subtracts the memory, it results in final values of transformation plasticity of 1.8×10^{-3} for the growth model and 2.45×10^{-3} for the random model. This difference in the behaviour between both models with regard to memory is due to the higher values of the cumulated equivalent plastic strain for the random model, as shown in the previous section.

However, the same parabolic shape for the evolution of transformation plasticity is retained, which is still very far from experience.

3.1.2. Viscous behaviour of the phases

Creep behaviour is introduced by adding an additional time-dependent inelastic strain to the elastic and plastic strains occurring in each phase, which satisfies a normality law. We consider secondary creep for which a widely used law is the Norton law [8, 9],

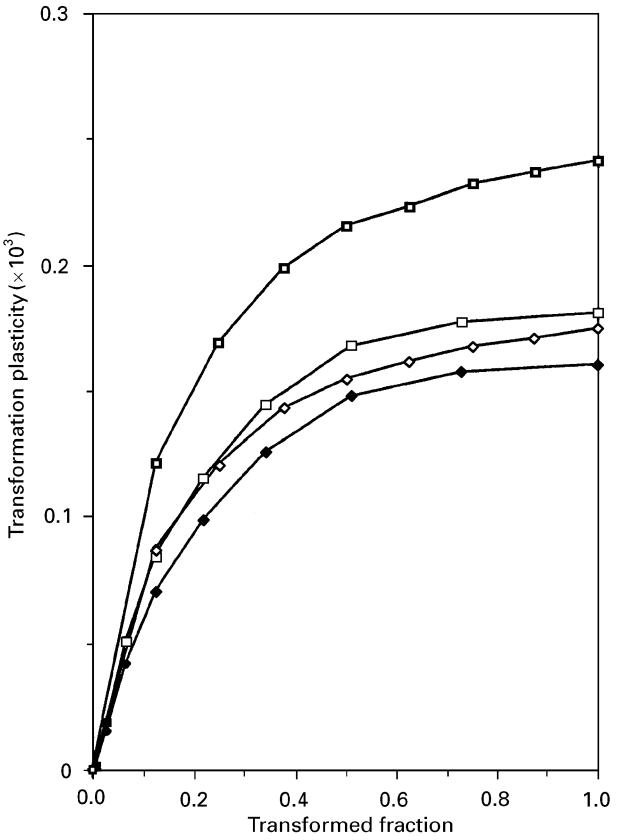

Figure 14 Evolution versus transformation progress of transformation plasticity for (■, □) random and (◇, ♦) spherical models, (□, ◆) with and (■, ◇) without plastic strain memory, "end" case at an applied stress of 20 MPa.

written

$$d\varepsilon^f = K\sigma_e^{m-1}\exp(-Q/RT)\boldsymbol{\sigma}^d\,dt \qquad (2)$$

in which $\boldsymbol{\varepsilon}^f$ is the creep strain, T the temperature, Q the activation energy, R the constant for perfect gases ($R = 8.32\,J\,mol^{-1}$). The coefficients K and m are specific to the material and to its conditions of use (temperature, deformation velocity range); they have been determined from experimental data [2] at the temperature of 673 °C for each phase. We consider a Johnson–Mehl–Avrami kinetic law of the form $x(t) = 1 - \exp(-bt^n)$. Coefficients b and n are identified from the transformation times corresponding to 10% and 90% transformed fractions, for an isothermal pearlitic transformation (673 °C) occurring under 20 MPa uniaxial stress. Creep properties and parameters of the kinetic law are given in Table II.

In the following, we consider the effect of creep for the spherical growth model, with properties imposed at the "end" of each transformation step and a uniaxial load of 20 MPa. We have imposed a total duration for the transformation of 120 s, corresponding to 90% transformed fraction (comparatively, the transformation of the nine first layers of elements represents 73% formed pearlite). Transformation plasticity is evaluated in the same way as for the non-viscous case, by subtracting at each step the elastic strain (due to the external load) and the transformation strain from the total strain.

TABLE II Creep data used in the simulation

Phase	Stress exponent, m	K ($MPa^{-m}\,s^{-1}$)
Austenite	1	3.6×10^{10}
Pearlite	2.55	4.05×10^{6}

Activation energy, $Q = 300\,000\,J\,mol^{-1}$
Kinetic law parameters: $n = 2$; $b = 1.56\times10^{-4}\,s^{-m}$

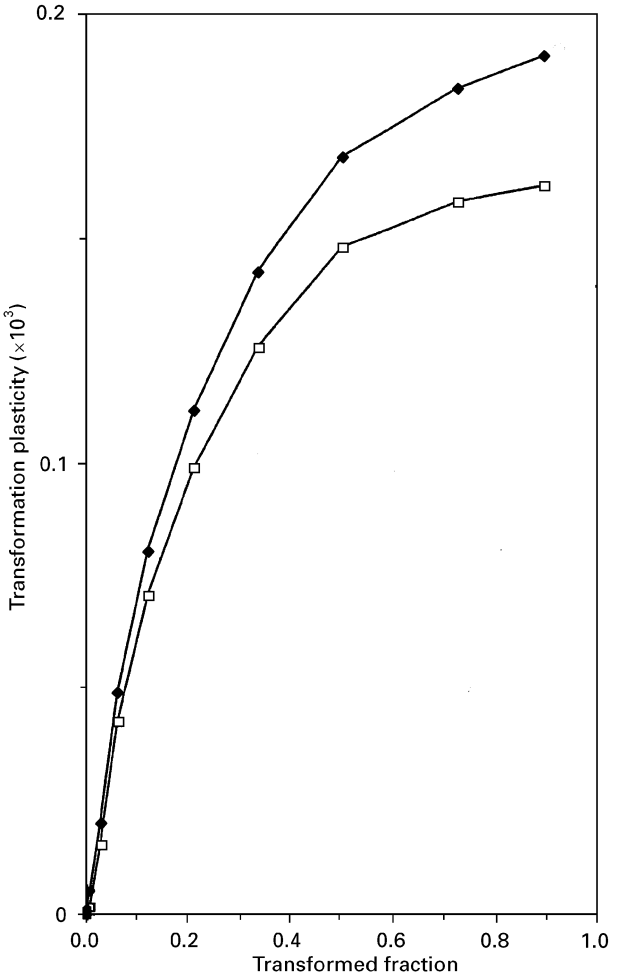

Figure 15 Evolution versus transformation progress of transformation plasticity for models (◆) with and (□) without creep: "end" case at an applied stress of 20 MPa. Total duration = 120 s.

We compare the evolutions of transformation plasticity (versus the transformed fraction) in both viscous and non-viscous cases (Fig. 15). The effect of creep is to increase gradually the transformation plastic strain (with respect to the non-viscous case); this is due to the fact that the creep contribution increases with the transformation progress. In order to obtain a better understanding of the effect of the creep contribution on transformation plasticity, we make a brief analysis of local strains developed during the transformation.

Fig. 16a–d show the evolutions of the equivalent cumulated plastic and creep strains for an "internal" node (node 3 3 3, Fig. 16a, b) and an "external" node (node 9 9 9, Fig. 16c, d); the sum of both strains is also

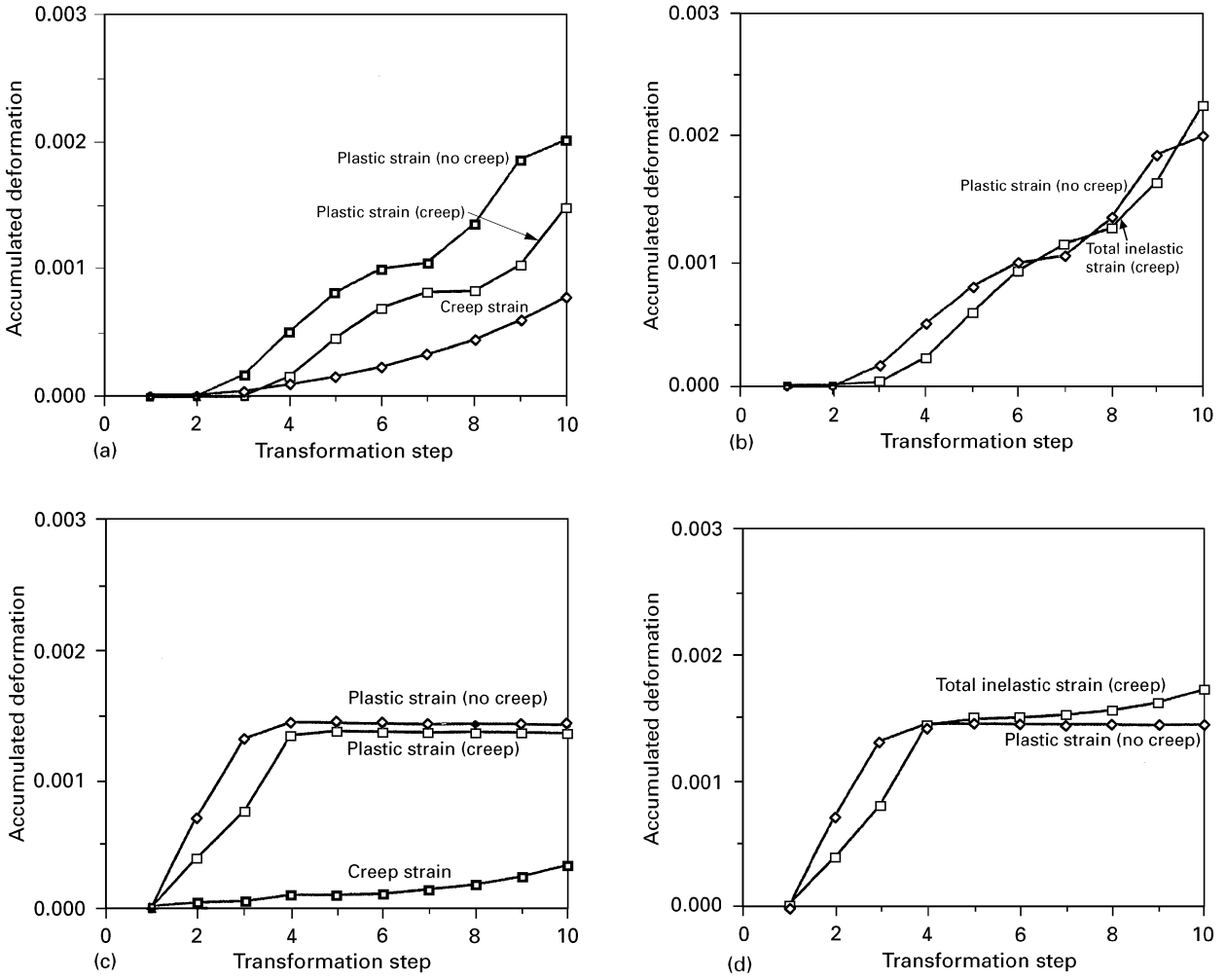

Figure 16 Evolution versus transformation progress of the accumulated plastic and creep strains for nodes (a, b) 3 3 3 and (c, d) 9 9 9 for an applied stress of 20 MPa.

shown on the same figure (ideally, it would have been preferable to represent the evolutions of the equivalent cumulated inelastic strain; we suppose, however, that the sum of both quantities gives a good representation of it), in order to compare the inelastic strains developed in viscous and non-viscous cases. Considering node 3 3 3, we observe similar values of plastic strains in both cases, with lower levels during the passage of the transformation front (between steps 2 and 3) when creep occurs, which can be related to stress relaxation. The difference in permanent strain at the "end" of the transformation (Fig. 16b) is due essentially to the development of a creep strain after transformation of the node (from step 6). Considering now node 9 9 9, the plastic strain is much smaller in the viscous case all along the transformation (at the end of the transformation, $\varepsilon_p = 1.5 \times 10^{-3}$ in the viscous case and $\varepsilon_p = 2 \times 10^{-3}$ in the non-viscous case) and the creep strain increases gradually with the transformation progress. As shown in Fig. 16d, the total inelastic strain developed when creep is considered is quite near the plastic strain of the non-viscous situation and the creep strain substitutes therefore partially for the plastic strain.

However, the introduction of creep does not lead to major changes of the resulting transformation plasticity evolution: the shape is still parabolic and the effect at the "end" of the transformation is only about 15%. It is therefore necessary to put forward other explanations of the discrepancy between simulation and experience. Previously [3] we particularly pointed out the difficulty of measuring the effective properties of the forming pearlite in its real conditions of deformation; those used in the simulation are those obtained for a stable sample (completely transformed) and properties of pearlite during its formation could be weaker, owing to a higher mobility of defects. In order to assess the effect of mechanical properties of pearlite, we consider an extreme case in which both phases have the same mechanical properties.

3.1.3. Effect of pearlite mechanical properties

Fig. 17 shows the evolution of transformation plastic strain for the spherical growth model, considering the cases of different and identical properties of the phases ("end" case, uniaxial load of 20 MPa). The evolution is quite similar at the beginning of the transformation (same initial slopes), and there is an increased discrepancy when the transformation advances, resulting in a large difference at the "end" (1.75×10^{-3} for

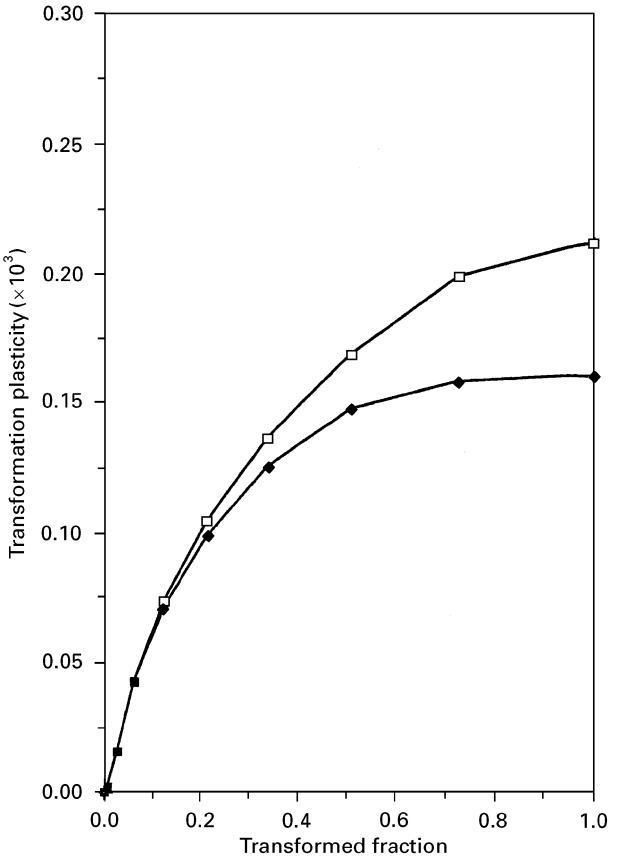

Figure 17 Evolution versus transformation progress of transformation plasticity for the spherical growth model. Effect of pearlite mechanical properties at an applied stress of 20 MPa, "end" case. (□) Same properties, (◆) different properties.

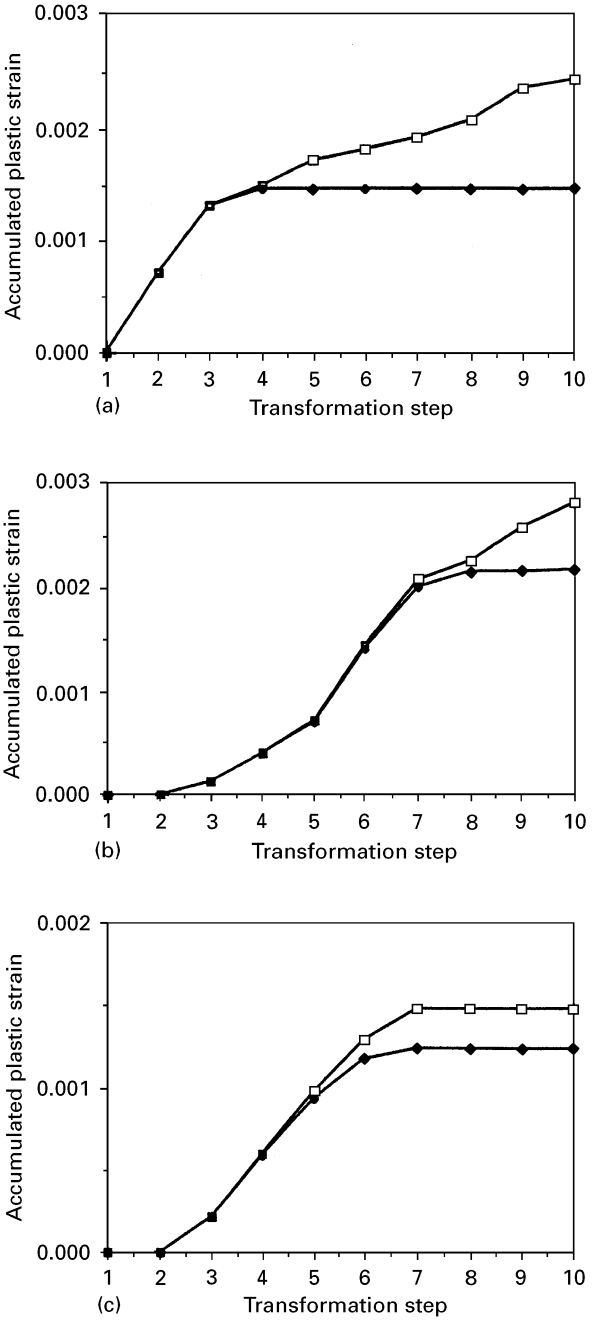

Figure 18 Spherical growth model for an applied stress of 20 MPa. Evolution versus transformation progress of the accumulated plastic strain for nodes (a) 3 3 3, (b) 7 7 7, (c) 11 11 11. Effect of pearlite mechanical properties. (□) Same properties, (◆) "end" case.

different properties; 2.17×10^{-3} for the same properties). These evolutions result from the local plasticity generated (Fig. 18): considering the evolution of ε_p for a given node on the diagonal, the same initial slopes are observed; when both phases have the same properties, plasticity continues to develop in already transformed nodes. A decrease in the slope can be noticed after transformation in that case, due to hardening for "internal" nodes (e.g. node 3 3 3), and to the effect of boundary conditions for "external" nodes (e.g. node 11 11 11). As a result, the non-linear evolution of transformation plasticity occurs when both phases have the same properties.

The effect of pearlite properties is quite different for the random progression model (Fig. 19). In that case, transformation plasticity develops in a more linear way and the "end" level is much higher (3.6×10^{-3} compared to 2.17×10^{-3} for the spherical growth description). The non-linear evolution obtained when the phases have different properties is due to the change of the environment of a transformed element, which contains a decreasing proportion of austenitic elements: it then becomes more difficult to plastify a volume in which the average mechanical properties increase with the transformation progress. This induces the observed saturation of transformation plasticity evolution.

When considering the discrepancy between both models when using the same properties of the phases, attention must be directed towards the transformation of the last layers of elements in the spherical growth model, which interact with the stiff boundary conditions applied to the cell; therefore, we investigated the influence of the way interactions between neighbouring cells are prescribed.

3.2. Description of interactions between neighbouring cells

Because the random progression model describes the physical reality at the macroscopic scale, there is no effect of the kind of boundary conditions applied to

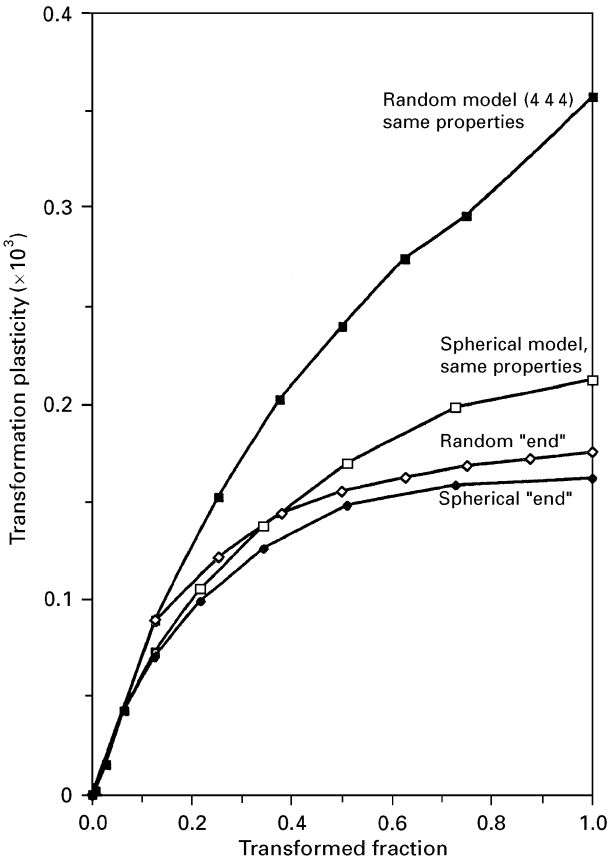

Figure 19 Evolution versus transformation progress of transformation plasticity for both models. Effect of pearlite mechanical properties at an applied stress of 20 MPa, "end" case.

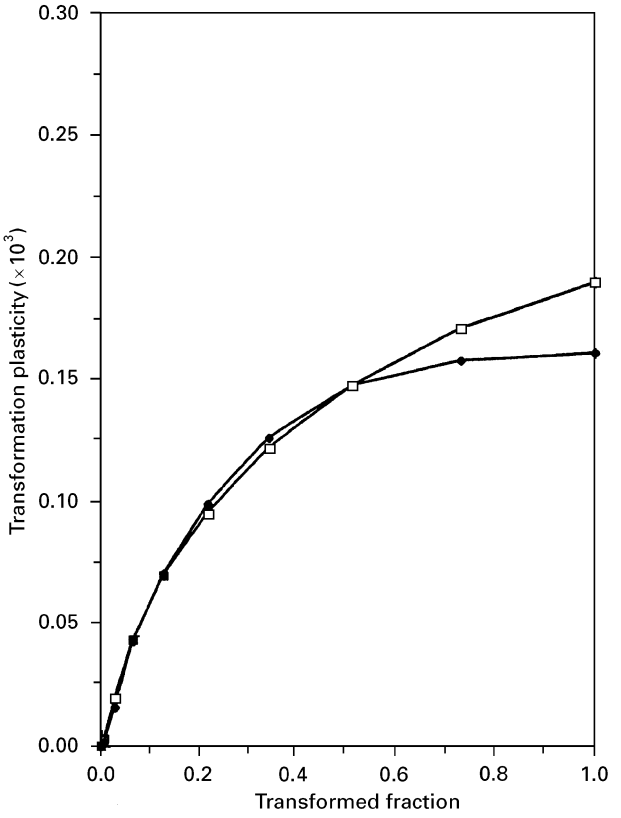

Figure 20 Spherical growth model. Evolution of transformation plasticity versus transformation progress; effect of boundary conditions at an applied stress of 20 MPa, "end" case. (□) Free boundaries, (◆) constrained boundaries.

the cell [3] and therefore we focus on the spherical growth description here.

The evolution of transformation plasticity obtained when considering rigid boundaries shows a saturation effect after about half-transformation, whatever the mechanical properties of the new phase. We explain this effect by the transformation of the last layers, which leads to less local plastic flow due to the presence of rigid boundaries. In order to investigate the effect of boundary conditions on transformation plasticity levels, we compare (Fig. 20) the evolution obtained with free boundaries to the original one ("end" case, 20 MPa applied load). The two curves are identical until half-transformation; afterwards, transformation plasticity develops more in the free case, owing to more local plastic flow.

In order to isolate the effect of boundary conditions from the additional effect of mechanical properties, we consider a simulation with free boundaries and identical properties of the phases. The evolutions of transformation plasticity obtained for the growth model with both kinds of boundary conditions are compared with that of the random description (Fig. 21). Considering the spherical model, there is a large effect of using free boundaries and the evolution is near linearity; moreover, the shape and levels reached are almost the same for both models (3.6×10^{-3}). This result shows that there is a strong effect of the kind of boundary conditions applied to the cell on the development of transformation plasticity. Further, it points out the importance of mechanical properties of pearlite, because this interaction effect is much weaker when pearlite has high properties.

In fact, the two kinds of boundary conditions used in the simulation describe two opposite situations: the free-boundary case corresponds to the absence of force coupling between adjacent cells, and the rigid-boundary case corresponds to the absence of displacement interactions between neighbouring cells. With respect to a physical situation in which the cell would represent a grain, using rigid boundaries seems realistic, because there is then a restriction of the plastic flow arising from the transformation of the material located near the grain surface. However, from the point of view of modelling, one could envisage less restrictive boundary conditions, still preserving periodicity but without symmetry, [10, 11] and which would allow the normal displacement to fluctuate on the boundary of the cell.

A further limitation of the actual description appears if one considers the crystallography of the transformation: depending on whether one describes a cubic (f c c) arrangement of atoms (actual situation of the model) or a hexagonal compact structure, there is a different choice of the appropriate cell, resulting in different topologies of the transformation progress and possibly in different transformation plasticity

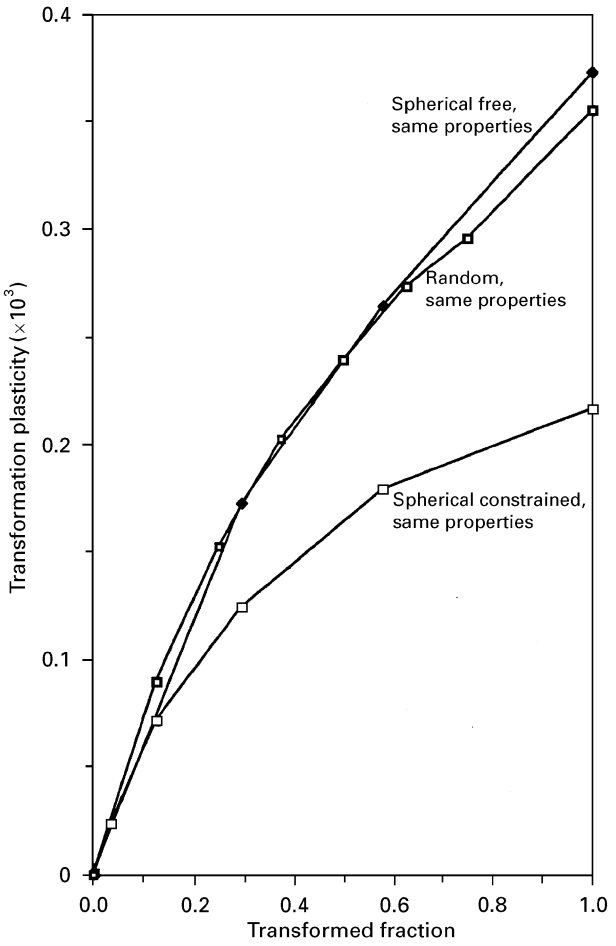

Figure 21 Evolution of transformation plasticity versus transformation progress for both models: effect of boundary conditions at an applied stress of 20 MPa, "end" case.

evolutions. Lastly, the difficulty of describing in a unified way (by the same model) both processes of nucleation and growth of the new phase, leads to the two scale-decoupled actual descriptions. The real transformation path (continuous nucleation and spherical growth) lies, in fact, between these two descriptions [3]. A further development of the simulation would then consist in a combination of both models into an integrated description of random germination of pearlite units and of their consecutive growth.

4. Conclusions

In the following conclusions, points 1–3 recall the partial conclusions of our previous two papers [3,4].

1. The random progression model is satisfactory from the numerical point of view, because only small effects of the transformation step, mechanical properties affectation and boundary conditions occur.

2. A good agreement was found between both descriptions, and the resulting transformation plastic strain is a strongly non-linear function of the new phase fraction. However, these calculated evolutions differ from the experimental behaviour, which is linear.

3. The application of the model to complex load-cases (multiaxial constant and uniaxial, which vary with the transformation progress) leads to a constitutive law for transformation plasticity, which is proportional to the external stress deviator. It can then be treated as an additional deformation in the behaviour law of the material at the macroscopic scale.

4. The analysis of the local results of the simulation has provided a guide for understanding, at least qualitatively, the evolutions of transformation plasticity. In particular, it has been shown that most of the deformation occurs inside and in the vicinity of the transforming layer.

5. All results obtained with different properties of the phases lead to an evolution of transformation plasticity with a saturation at the "end" of the transformation, whatever the description of the transformation. As the behaviour law of the phases (loss of memory of hardening, creep behaviour) becomes more complex, it leads to increased transformation plasticity making it closer to the experimental results. However, the values obtained at the beginning of the transformation are too high.

6. By considering the growth description, simulations with identical properties of the phases and free boundaries have clearly evinced the effect of rigid boundary conditions, which induce lower plasticity of the boundary layers. There is an additional effect of the properties of pearlite: simulations with identical properties of the phases lead to a transformation plastic strain shape similar to those found experimentally, although the levels are higher in the simulation ($3.6 \times 10^{-3}/2.9 \times 10^{-3}$). These results lead us to suppose that pearlite should be more plastically deformed: they can be correlated to the results of Liebaut [12] who performed simulations of the behaviour law of the material at the "macroscopic scale". When considering transformation plasticity (as an additional term), such simulations overestimated the measured yield stress after 60% transformation. Further investigations concerning the mechanical properties of the forming pearlite would be necessary, because they could be weaker than that considered in the simulation, owing to a greater mobility and density of defects.

Acknowledgements

The authors thank STU (National Swedish Board for Technical Development) and CNRS (Centre National de la Recherche Scientifique), who sponsored this work.

References

1. E. GAUTIER, A. SIMON and G. BECK, *Acta Metall.* **35** (1987) 1367.
2. S. DENIS, E. GAUTIER, A. SIMON and G. BECK, *Mater. Sci. Technol.* **1** (1985) 805.
3. J. F. GANGHOFFER, S. DENIS, E. GAUTIER, A. SIMON and S. SJÖSTRÖM, *Eur. J. Mech. A* **12** (1993) 21.

4. *Idem*, *ibid*. **13** (1994) 803.
5. J. B. LEBLOND, *J. Mech. Phys. Solids* **34** (1986) 395.
6. B. RANIECKI, *Mater. Sci. Technol.* **1** (1985) 857.
7. J. B. LEBLOND, *Int. J. Plasticity* **5** (1989) 573.
8. J. L. CHABOCHE and J. LEMAITRE, "Mécanique des matériaux solides" (Dunod, Paris, 1985).
9. P. POIRIER, "Plasticité à haute température des solides cristallins" (Eyrolles, Paris, 1976).
10. A. ZAOUI, "Homogeneization techniques in composite media", Lecture Notes in Physics, no. 243 (Paris, 1983).
11. J. SANCHEZ-HUBERT and E. SANCHEZ-PALENCIA, "Introduction aux méthodes asymptotiques et à l'homogénéisation" (Masson, Paris, 1992).
12. C. LIEBAUT, E. GAUTIER and A. SIMON, Mechanical behaviour of an Fe–0.2C steel during transformation, Proceedings THERMEC 88, I.S.I.J, Ed. I., (Tamura, 1988).

Received 8 December 1995
and accepted 10 March 1997